Early Stage Spinodal Decomposition in Polymer Solution under High Pressure

Jun'ichi Kojima,[†] Mikihito Takenaka,[‡] Yoshiaki Nakayama,[†] and Takeji Hashimoto*,[‡]

Asahi Chemical Industry Co. Ltd., Nobeoka, Miyazaki 882-0031, Japan, and Department of Polymer Chemistry, Graduate School of Engineering, Kyoto University, Kyoto 606-8501, Japan

Received May 20, 1998; Revised Manuscript Received January 26, 1999

ABSTRACT: Early stage spinodal decomposition (SD) of polymer solutions (polypropylene/trichlorofluoromethane) induced by pressure jump was investigated with a light scattering instrument designed for polymer solutions under high pressure and high temperature. The changes in the scattered intensity with time at the early stage SD were found to be approximated by Cahn linearized theory or Cahn−Hilliard−Cook theory. The analyses with the theories yielded the characteristic parameters such as the interdiffusion coefficient D_{app} and the characteristic wavenumber $q_m(0)$. Unlike other experiments on the polymer solutions, the pressure dependence of the parameters was found to obey the mean field behavior. This may be because the quench depth conditions attained by the pressure jump were much deeper than those attained in other experiments.

I. Introduction

Supercritical fluids have been used as superior media in the processing of polymers such as fractionation, purification, polymerization, and precipitation,[1] since their density and solubility are those of liquid while their transport properties are those of gas and the phase behavior of their solution is easily controlled by changing temperature and pressure. To improve the processing, the phase diagrams of polymer/(nearly) supercritical fluid systems have been studied extensively.[2−7] However, there are no studies on the dynamics of phase separation processes in polymer/(nearly) supercritical fluid systems even though the dynamical properties of the phase separation processes are important in the formation of particles and fibers of polymers.

As reported in our previous paper,[8] we have developed a light scattering instrument that is specially designed for polymer solutions under high temperature and high pressure to investigate the phase separation processes induced by pressure jump. We, then, explored the following physical properties in polypropylene (PP)/trichlorofluoromethane (CCl_3F) under high pressures and high temperatures: (1) We measured the cloud point curve of PP/CCl_3F as a function of temperature T and pressure P so that the phase diagram was found to exhibit a lower critical solution temperature type and an upper critical solution pressure type; (2) The preliminary observation of the changes in the light scattering profiles with time during the phase separation processes of PP/CCl_3F induced by pressure jumps suggests that the phase separation process at deeper pressure quenches progresses via spinodal decomposition (SD).

In this paper, we will focus on the early stage SD in PP/CCl_3F. Many experimental results on the SD of polymer blends or polymer solutions support that the early stage SD can be approximated by the linearized theory[9−26] as will be described in section II. Here we will test the validity of the linearized theory for the early stage SD in PP/CCl_3F under high pressures and high temperatures.

Usually, the experiments on the phase separation of binary fluids have been carried out at very shallow quench conditions, because the deep quench conditions cannot be easily attained either by the temperature-jump (T-jump) (as the deep quenches by T-jump are generally slow compared with rates of phase separations at deep quenches) or the pressure-jump experiments involving a small pressure changes.[27−29] However, we can attain a precise pressure jump up to 1 MPa quickly so that we can measure the dynamics of phase separation processes at deep quench conditions with this instrument. We will, thus, compare the results at deep quenches with those at shallow quenches.

The linearized SD theory will be described in section II. We will show the experimental results in section IV after describing the light scattering instrument, the samples, and the quench depth conditions in section III. Section V will present the results of the critical test of the linearized theory for the solution. We will analyze the quench depth dependence of the characteristic parameters for the early stage SD in section VI. Finally, we will summarize our results in section VII.

II. Linearized Theory

The dynamics of phase separation processes in A/B binary mixtures is described by time-dependent Ginzburg−Landau theory for the local concentration fluctuation $\delta\phi_A(\mathbf{r},t)$ at position $\mathbf{r}$ and time t:[30,31]

$$\frac{\partial}{\partial t}\delta\phi_A(\mathbf{r},t) = \Lambda\nabla^2\mu(\mathbf{r},t) + \zeta(\mathbf{r},t) + (\text{HD term}) \quad (1)$$

where Λ is the Onsager kinetic coefficient, $\mu(\mathbf{r},t)$ is the local chemical potential, $\zeta(\mathbf{r},t)$ is the random thermal force term, and the HD term is the long-range hydrodynamic interaction.[30,31] $\delta\phi_A(\mathbf{r},t)$ is given by

$$\delta\phi_A(\mathbf{r},t) \equiv \phi_A(\mathbf{r},t) - \phi_{A0} \quad (2)$$

* To whom correspondence should be addressed.
[†] Asahi Chemical Industry Co. Ltd.
[‡] Kyoto University.

10.1021/ma980799n CCC: $18.00
Published on Web 03/05/1999

with $\phi_A(\mathbf{r},t)$ and ϕ_{A0} being respectively the volume fraction of the A component at $\mathbf{r}$ and t and the space-averaged $\phi_A(\mathbf{r},t)$. The random thermal force term can be expressed by the following fluctuation−dissipation relation:[32]

$$\langle \varsigma(\mathbf{r},t)\, \varsigma(\mathbf{r}',t')\rangle = -2k_B T\Lambda\nabla^2\delta(\mathbf{r}-\mathbf{r}')\,\delta(t-t') \quad (3)$$

where k_B and T are respectively the Boltzmann constant and absolute temperature, and $\langle\ \rangle$ denotes thermal average. If $\delta\phi_A(\mathbf{r},t)$ is small and the HD term can be neglected, eq 1 can be linearized in terms of $\delta\phi_A(\mathbf{r},t)$:

$$\frac{\partial}{\partial t}\delta\phi_A(\mathbf{r},t) = \Lambda\nabla^2(-\tau - K\nabla^2)\delta\phi_A(\mathbf{r},t) + \zeta(\mathbf{r},t) \quad (4)$$

where K is a positive constant, and τ is positive in unstable region and increases with the quench depth.

By applying Fourier transformation to eq 4, we obtain

$$\frac{\partial}{\partial t}\delta\phi_A(q,t) = -\Lambda q^2(-\tau + Kq^2)\delta\phi_A(q,t) + \zeta(q,t) \quad (5)$$

where q is wavenumber, and $\delta\phi_A(q,t)$ and $\zeta(q,t)$ are respectively the q-Fourier mode of ϕ_A and ζ. We can solve eq 5 in terms of the structure factor $S(q,t)$ $[=\langle|\delta\phi_A(q,t)|^2\rangle]$[33]

$$S(q,t) = S(q,\infty) + [S(q,0) - S(q,\infty)]\exp[2R(q)t] \quad (6)$$

where $S(q,0)$, $S(q,\infty)$, and $R(q)$ are respectively $S(q,t)$ at $t = 0$, the virtual structure factor due to the random thermal force effects, and the growth rate for $\delta\phi_A(q,t)$. $R(q)$ is expressed by

$$R(q) = D_{app}q^2\left[1 - \frac{q^2}{2q_m^2(0)}\right] \quad (7)$$

where D_{app} and $q_m(0)$ are respectively the interdiffusion coefficient and the characteristic wavenumber for the concentration fluctuations developed in the early stage SD. They are given by

$$D_{app} = \Lambda\tau \quad (8)$$

and

$$q_m(0) = \sqrt{\frac{\tau}{2K}} \quad (9)$$

For a large quench depth, the random thermal force effects are negligible at $q \ll \sqrt{2}q_m(0)$, and the time change in $S(q,t)$ is expressed by

$$S(q,t) = S(q,0)\exp[2R(q)t] \quad (10)$$

Cahn[34] first derived the linearized theory without the random thermal force effects (eq 10). Cook,[33] then, introduced the random thermal force effects into the linearized theory (eq 6). Hereafter we refer to the linearized theory with and without the random thermal force effects as Cahn−Hilliard−Cook theory (CHC theory) and Cahn theory, respectively. The theories will be compared with the experimental results in section IV.

III. Experimental Section

A. Light Scattering Instrument. As described in our previous paper,[8] the light scattering instrument used in this study has the following features: (1) the instrument withstands up to pressure 34.3 MPa and temperature 573 K; (2) viscous polymer solutions can be easily handled; (3) pressure jump can be attained with 0.01 MPa precision; and (4) the scattered intensity distribution over wide angular range (0°−30° in the air) can be measured at 100 scans/s by using the photodiode array light scattering system. We describe below only the essential part of the apparatus for this work, and the details should be referred to ref 8.

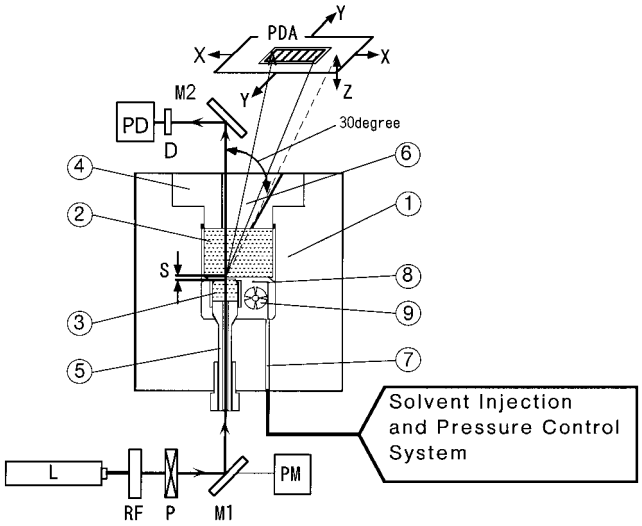

Figure 1. Block diagram of light scattering instruments: L, laser; RF, rotating circular neutral density filter; P, polarization rotator; M1 and M2, mirror; PM, monitor photodiode; S, sample thickness; PDA, photodiode array; D, diffuser; and PD, photodiode as a transmittance detector.

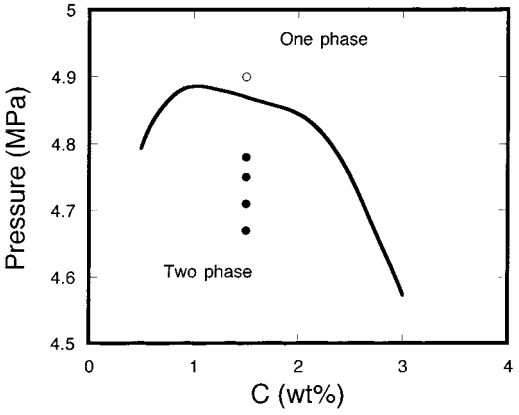

Figure 2. Cloud point curve at $T = 452.5$ K for PP/CCl_3F solution. Filled circles and open circle respectively indicate points after and before quench.

Figure 1 shows a whole block diagram of the light scattering instrument. The light scattering cell is connected to the pressure control system which controls the pressure in the cell and the magnitude of pressure jump. The pressure and temperature in the cell are measured by a pressure gauge and a RTD temperature sensor, respectively. A 20 mW He−Ne laser (L) (wavelength $\lambda = 632.8$ nm in air) is used as a light source. After the intensity and polarization plane of the beam from the laser are adjusted by a rotating circular neutral density filter (RF) and a polarization rotator (P), respectively, the beam is reflected by a mirror (M1) and introduced into the sample (S) in the cell. A portion of the beam passes through the mirror M1 and is detected by a monitor photodiode (PM) which monitors the fluctuation of the incident beam intensity. The scattered intensity is detected by the photodiode array (PDA) with 35 elements (Hamamatsu Photonics S2312-35Q). The turbidity of the sample is monitored by measuring the incident beam through the samples with a photodiode (PD).

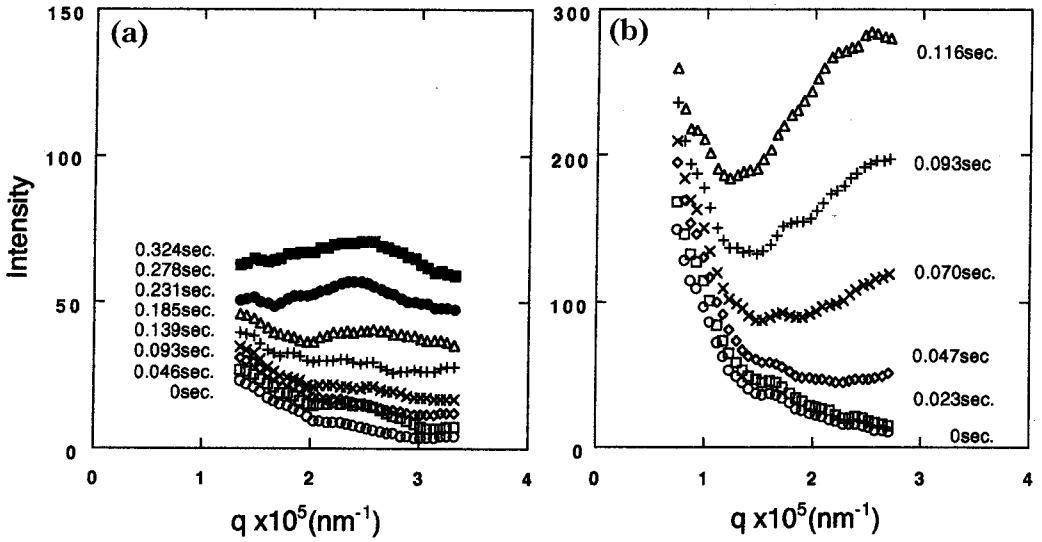

Figure 3. Changes in the light scattering profiles with time during early stages in the phase separation process after the pressure drop to $P = 4.78$ (a) and 4.67 MPa (b) at $T = 452.5$ K.

The personal computer controls the PDA and simultaneously collects the outputs of the photodiode array, the monitor photodiode, the transmittance, the RTD sensor, and the pressure gauge. The details of the instrument are described in our previous paper.[8]

B. Sample Preparation and Quench Condition. The polymer and solvent used here are respectively PP (weight-average molecular weight $M_w = 3.5 \times 10^5$, $M_w/M_n = 6.5$, M_n: number-average molecular weight) and CCl_3F. Figure 2 shows the phase diagram of the polymer solutions at 452.5 K. The phase diagram is an upper critical solution pressure type, and the regions above and below the cloud point curve are one-phase and two-phase regions, respectively. It should be noted that the phase diagram exhibits one peak at $c = 1.0$ wt % and one shoulder at $c = 2.1$ wt %. This shape is due to the polydispersity of PP ($M_w/M_n = 6.5$) and the concentration dependence of the χ parameter, as seen, for example, in the work of Koningsveld et al.[35] for diphenyl ether solution of polystyrene with a molecular weight polydispersity. The polymer solution containing 1.5 wt % of the polymer was used for this study. We stirred the polymer solution at 453 K and 10 MPa for 30 min to make the solution homogeneous and then kept the solutions at $T = 452.5$ K and $P = 4.90$ MPa before we quenched the solution from $P = 4.90$ (corresponding to a point shown by the open circle in Figure 2) to 4.78 ($\Delta P = 0.1$), 4.73 ($\Delta P = 0.15$), 4.71 ($\Delta P = 0.17$), and 4.67 MPa ($\Delta P = 0.21$), where $\Delta P = P_c - P$ with the cloud point pressure $P_c = 4.88$ MPa. These pressures are shown by the filled circles in Figure 2.

The changes in the scattered intensity $I(q,t)$ [$=CS(q,t)$, $C =$ constant] at t and q after the onset of the pressure jumps with time were measured by the photodiode array light scattering system. The scattered intensity was corrected for the fluctuation of the incident beam and the turbidity of the sample.[36] The vapor−liquid equilibrium pressure at $T = 452.5$ K is 3.60 MPa.

IV. Experimental Results

Figure 3 shows the changes in the light scattering profiles with time during the phase separation process after the pressure drop from $P = 4.90$ MPa to $P = 4.78$ (part a) and 4.67 MPa (part b). In both parts we plotted the scattered intensity as a function of q defined by

$$q = (4\pi/\lambda)\sin(\theta/2) \tag{11}$$

where λ and θ are respectively the wavelength of the incident beam and the scattering angle in the solution. As time elapses, the scattered intensity increases with time at observed q region; subsequently, the peak in the scattered intensity appears at high q region in both cases. The change at $P = 4.67$ MPa, however, is much faster than that at $P = 4.78$ MPa, and the q value at the peak position at $P = 4.78$ MPa is smaller than that at $P = 4.67$ MPa, because the quench depth at $P = 4.67$ MPa is deeper than that at $P = 4.78$ MPa.

V. Test of the Linearized Theory

Figure 4 shows the semilogarithmic plot of $I(q,t)$ vs t at various fixed q after the pressure drop from $P = 4.90$ MPa to $P = 4.73$ (part a), 4.71 (part b), and 4.67 MPa (part c). Each part shows the linear relationship between $\ln[I(q,t)]$ vs t at an early time region, indicating that the time evolution of the structure factor can be expressed by Cahn's theory or eq 10 and that the random thermal force effects are negligible at the observed q region for the three quench experiments. We estimated $R(q)$ from the slope of the plot to obtain the characteristic parameters or D_{app} and $q_m(0)$. In the case of the shallowest quench or $P = 4.78$ MPa, we, however, did not find the linear relationship in $\ln[I(q,t)]$ vs t, though we do not show the plot here. This is because the thermal noise effects cannot be negligible. We, hence, applied the 1/3 power plot[37] to the time change in the scattered intensity affected by the thermal noise effects to estimate $R(q)$. According to Sato and Han, after expanding the exponential part in eq 6 and rearranging, we obtain

$$\left[\frac{t}{I(q,t) - I(q,0)}\right]^{1/3} = \frac{1}{[2(I(q,0) - I(q,\infty))R(q)]^{1/3}} \times \left\{1 - \frac{1}{3}R(q)t + \frac{1}{81}[R(q)t]^3 \ldots\right\} \tag{12}$$

If eq 12 can describe the phase separation process at $R(q)t < 1$, the plot of $[t/\{I(q,t) - I(q,0)\}]^{1/3}$ vs t becomes linear, and we can estimate $R(q)$ from the slope and the intercept of the plot. The plot for the phase separation at $P = 4.78$ MPa shows a good linearity as shown in Figure 5 from which $R(q)$ was estimated. Here it should be noted that the time domain where a linearity between $\ln[I(q,t)]$ and t or that between $[t/\{I(q,t) - I(q,0)\}]^{1/3}$ and t holds should become narrower with increasing $R(q)$, and hence with increasing q and quench

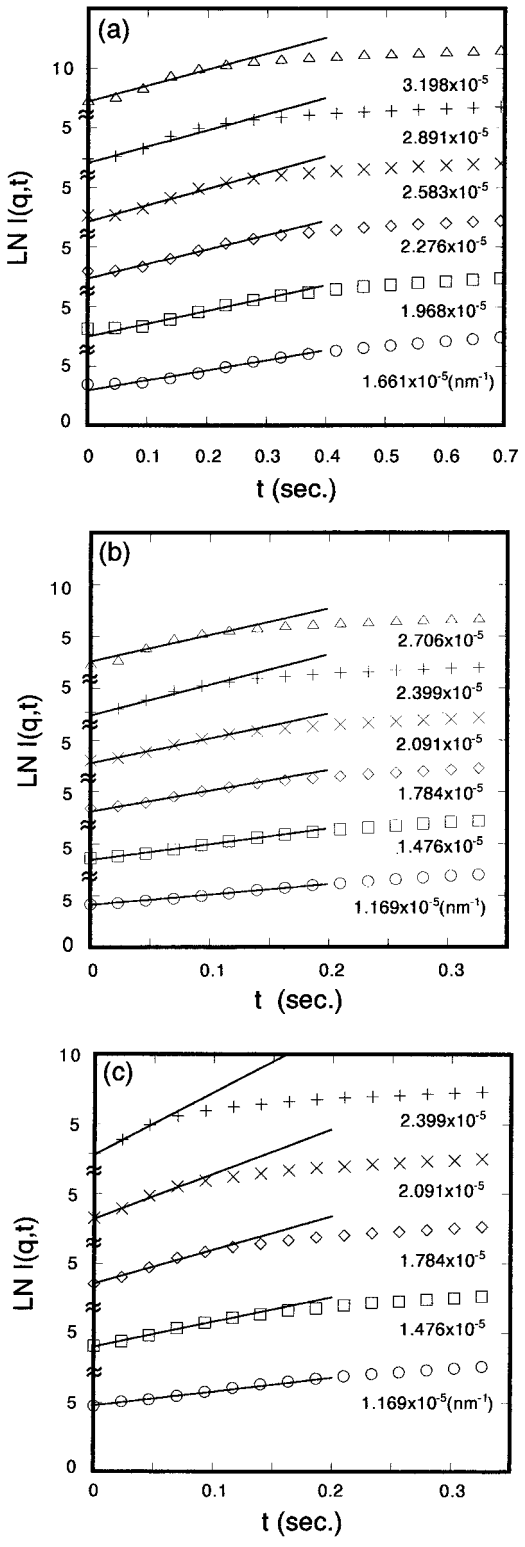

Figure 4. Semilogarithmic plot of $I(q,t)$ vs t at various fixed q after the pressure drop to $P = 4.73$ (a), 4.71 (b), and 4.67 MPa (c) at $T = 452.5$ K.

depth under the experimental conditions covered in this experiment, since the nonlinear effects due to the increase of the amplitude of the concentration fluctuations appear at an earlier time domain. We made, thus, the time domain narrower with increasing $R(q)$ to reduce the nonlinear effects on estimating $R(q)$. We plotted $R(q)/q^2$ as a function of q^2 for the four quench experiments to evaluate D_{app} and $q_m(0)$ from the intercept and slope in Figure 6. Each plot shows the linearity

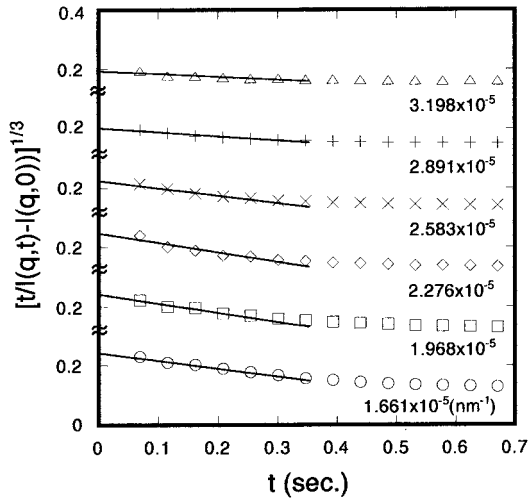

Figure 5. The 1/3 plot at various fixed q after the pressure drop to $P = 4.78$ MPa at $T = 452.5$ K.

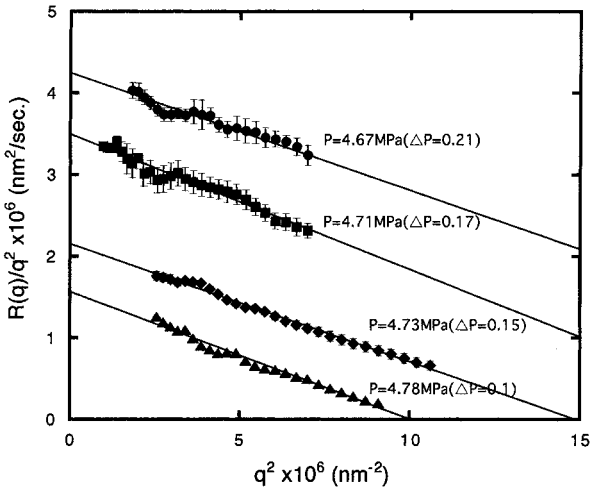

Figure 6. $R(q)/q^2$ vs q^2 plots for each quench specified in the figure.

Table 1. Characteristic Parameters in Early Stage SD

P (MPa)	$D_{app} \times 10^{-6}$ (nm^2/s)	$q_m(0) \times 10^3$ (nm^{-1})	$\Lambda_m \times 10^{-3}$ (nm)	t_c (s)
4.78	1.57 ± 0.03	2.24 ± 0.04	2.80	0.126
4.73	2.16 ± 0.01	2.73 ± 0.02	2.30	0.062
4.71	3.50 ± 0.13	3.25 ± 0.12	1.93	0.027
4.67	4.23 ± 0.16	3.84 ± 0.15	1.64	0.016

as described by eq 7 within the experimental accuracy. The validity of eq 6 or eq 10 for the time changes in the scattered intensity and the linear relationship between $R(q)/q^2$ and q^2 indicate that the dynamics of the early stage SD in PP/CCl_3F can be approximated by the linearized theory.

VI. Quench Depth Dependence of Characteristic Parameters

Table 1 summarizes the characteristic parameters obtained from $R(q)/q^2$ vs q^2 plots in the early stage SD for the four quench experiments. Here the characteristic wavelength Λ_m and the characteristic time t_c are defined by

$$\Lambda_m \equiv \frac{2\pi}{q_m(0)} \tag{13}$$

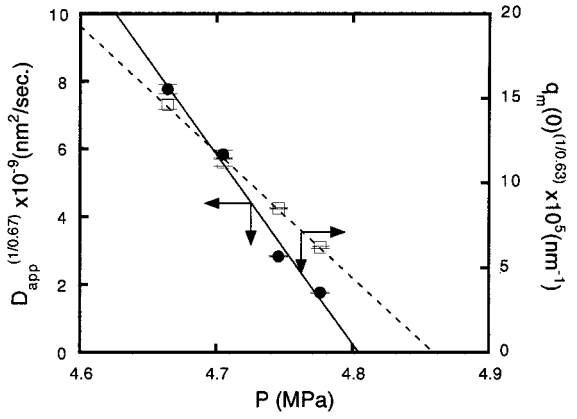

Figure 7. $[q_m(0)]^{1/0.63}$ and $[D_{app}]^{1/0.67}$ plotted as a function of P.

and

$$t_c \equiv \frac{1}{D_{app} q_m^{\,2}(0)} \tag{14}$$

respectively.

If the system obeys the 3D kinetic Ising model,[38] the quench depth dependencies of D_{app} and $q_m(0)$ are given by

$$D_{app} = D_0 \epsilon^{0.67} \tag{15}$$

and

$$q_m(0) = q_{m0} \epsilon^{0.63} \tag{16}$$

respectively. Here ϵ characterizes the quench depth and is defined by

$$\epsilon \equiv \frac{|T - T_s|}{T_s} \tag{17}$$

with T_s being T at the spinodal point. For the quench induced by pressure jump, ϵ is given by

$$\epsilon \equiv \frac{|P - P_s|}{T_s}\left(\frac{\partial T}{\partial P}\right)_s \tag{18}$$

where P_s is P at the spinodal point, and $(\partial T/\partial P)_s$ is the value $(\partial T/\partial P)$ at the spinodal point. It should be noted that the critical exponent for D_{app} in eq 15 can be obtained by using the mode coupling theory,[39] because the system near critical point is affected by the hydrodynamic interactions, which is neglected in CHC theory. Lal et al.[28] and Kuwahara et al.[29] reported that the exponents obtained for a polystyrene (PS)/cyclohexane (CH) system and a poly(dimethylsiloxane)/diethyl carbonate system, respectively, agrees with those of the 3D kinetic Ising model.

We plotted $[q_m(0)]^{1/0.63}$ and $[D_{app}]^{1/0.67}$ as a function of P in Figure 7 to check whether the PP/CCl_3F obeys the 3D kinetic Ising model. The plots of $[q_m(0)]^{1/0.63}$ and $[D_{app}]^{1/0.67}$ vs P for the PP/CCl_3F show linearity as observed for other experiments.[28,29] However, the pressure at the spinodal point $P_s = 4.86$ MPa estimated by the extrapolation of the plots of $[q_m(0)]^{1/0.63}$ vs P to $[q_m(0)]^{1/0.63} = 0$ does not agree with $P_s = 4.81$ MPa obtained from the plot of $[D_{app}]^{1/0.67}$ vs P, indicating that the system does not obey the 3D kinetic Ising model.

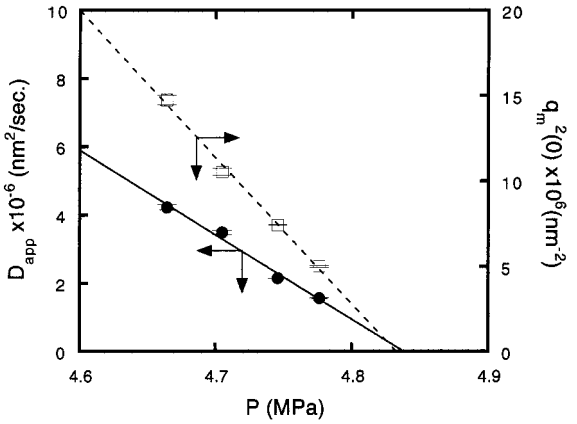

Figure 8. $q_m^{\,2}(0)$ and D_{app} plotted as a function of P.

According to the mean field theory,[40] τ in eq 4 is given by

$$\tau = A\epsilon \tag{19}$$

where A is a positive constant. Substituting eq 19 into eqs 8, 9, and 18, we obtained

$$D_{app} = \Lambda A \epsilon \sim |P - P_s| \tag{20}$$

and

$$q_m(0) = \left(\frac{A\epsilon}{2K}\right)^{0.5} \sim |P - P_s|^{0.5} \tag{21}$$

In Figure 8, D_{app} and $q_m^{\,2}(0)$ are plotted as a function of P. Both plots show the linear relationship, which indicates that the early stage SD in the PP/CCl_3F obeys the mean field theory. We can determine the spinodal pressure P_s by extrapolating the plots of D_{app} and $q_m^{\,2}(0)$ vs P to zero. $P_s = 4.81_5$ and 4.82_3 MPa are obtained from $q_m^{\,2}(0)$ vs P and D_{app} vs P, respectively, and both values of P_s agree within experimental error. Thus, the mean-field model predicts our experiments better than the 3D kinetic Ising model.

The discrepancy between our result and the results by Kuwahara et al. and Lal et al. in terms of the critical exponents of D_{app} and $q_m(0)$ is due to the fact that the quench depth of our experiment is much deeper than those of their experiments. The quench depth employed by Kuwahara et al. varies from $\epsilon = 6.8 \times 10^{-6}$ to 47.1×10^{-6}, and that by Lal et al. is up to $\epsilon = 4.2 \times 10^{-3}$. ϵ calculated by using eq 18 with $P_s = 4.85$ MPa for our system is from 0.014 for $P = 4.78$ MPa and 0.037 for $P = 4.67$ MPa. Therefore, the values of ϵ for our experiment are about 1000 times as large as those of Kuwahara et al. and about 10 times as large as those of Lal et al., indicating that our experimental condition is far from the critical region. Actually, the values of D_{app} and $q_m(0)$ of our experiment are much larger than those of them. To the best of our knowledge, it is the first time that the mean field behavior is observed in the dynamics of the phase separation processes via SD for polymer solutions. It should be noted that the quick, large pressure jump and the quick scan of the scattered intensity with the photodiode array light scattering system enable us to measure the very fast processes associated with the deep quench and hence to detect the mean-field behavior in the phase separation dynamics of polymer solutions.

We compare the experimental values of $q_m(0)_{exp}$ and the theoretical ones of $q_m(0)_{theor}$. According to Schichtel and Binder,[41] $q_m(0)$ for polymer solution with polydisperse polymer in the context of the mean field theory is given by

$$q_m(0) = 3\left[\frac{\frac{1}{N_w\phi_P} + \frac{1}{\phi_S}}{\frac{N_z a_P^2}{N_w\phi_P} + \frac{a_S^2}{\phi_S}}\right]^{0.5} \epsilon_\chi^{0.5} \tag{22}$$

where N_w and N_z are respectively weight-average and z-average polymerization indices; a_i and ϕ_i are respectively the segment length and the volume fraction of the ith component, which is either solvent denoted by subscript (S) or polymer (P). ϵ_χ is defined by

$$\epsilon_\chi = \frac{\chi - \chi_S}{\chi_S} \tag{23}$$

where χ and χ_S are respectively the Flory−Huggins segmental interaction parameter between polymer and solvent and χ at the spinodal point given by

$$\chi_s = \frac{1}{2}\left(\frac{1}{N_w\phi_P} + \frac{1}{\phi_S}\right) \tag{24}$$

If we assume that the statistical segment length of CCl_3F, a_{CCl_3F}, is identical with the segment length of PP, $a_{PP} = 0.570$ nm,[42] and that the molecular weight distribution of PP can be approximated by a logarithmic normal distribution[43] so that $M_z/M_w = M_w/M_n = 6.5$, we obtain

$$q_m(0)_{theor} = 0.255\epsilon_\chi^{0.5} \tag{25}$$

in units of nm^{-1}. Here we used $\phi_S = 0.985$ calculated with the density of PP ($\rho_{PP} = 0.91$) and that of CCl_3F ($\rho_{CCl_3F} = 0.93$). ρ_{CCl_3F} and ρ_{PP} are obtained from the result of the PVT measurement of CCl_3F at 3.4 MPa and 452 K and taken from the *Polymer Handbook*,[42] respectively.

On the other hand, to calculate ϵ_χ for the pressure jump, we calculated the P dependence of χ between PP and CCl_3F from the phase diagram of the solution at T = 453 K (see Figure 7c in ref 8) and then obtained

$$\chi = A + B/P \tag{27}$$

with A and B being 0.372 and 0.684, respectively. We can estimate ϵ_χ for the pressure jump from the following equation:

$$\epsilon_\chi = \frac{B}{\chi_s}\left(\frac{1}{P} - \frac{1}{P_s}\right) \tag{28}$$

We plotted $q_m(0)$ as a function of $\epsilon_\chi^{0.5}$ in Figure 9, and the results give

$$q_m(0)_{exp} = (0.0348 \pm 0.0006)\epsilon_\chi^{0.5} \tag{29}$$

in units of nm^{-1}, indicating that the values of $q_m(0)_{exp}$ are smaller than those of $q_m(0)_{theor}$ by a factor of 7.3.

To check whether such a discrepancy between $q_m(0)_{exp}$ and $q_m(0)_{theor}$ is unique to our system or whether it can be found in other polymer/nonsuprecritical-fluid systems, we also compared $q_m(0)_{exp}$ with $q_m(0)_{theor}$ for the PS/CH ($M_{w,PS} = 2.33 \times 10^5$, polymer concentration c = 7 wt %) by Lal et al.[28] We used the following expression to calculate $q_m(0)_{theor}$ for the PS/CH:

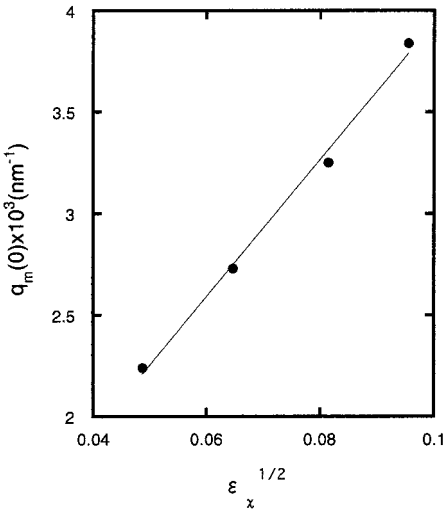

Figure 9. $q_m(0)$ plotted as a function of $\epsilon_\chi^{0.5}$.

$$q_m(0) = 3\left[\frac{\frac{1}{N_w\phi_P} + \frac{1}{\phi_S}}{\frac{N_z a_P^2}{N_w\phi_P} + \frac{a_S^2}{\phi_S}}\right]^{0.5} \epsilon_\chi^{2/3} \tag{30}$$

Here we assume that the front factor of $q_m(0)_{theor}$ ([ ] in eq 22) is valid in the critical region of the solution but that the critical exponent of ϵ_χ for $q_m(0)$ is not 0.5 but 2/3. We, then, obtained

$$q_m(0)_{theor} = 12.25\epsilon_\chi^{2/3} \tag{31}$$

Since Lal et al. did not plot $q_m(0)_{exp}$ vs $\epsilon_\chi^{2/3}$ in their paper, we calculated the temperature dependence of ϵ_χ by using the temperature dependence of χ for PS/CH system given by[44]

$$\chi = 0.203 + 90.65/T + 0.3092\phi + 0.1554\phi^2 \tag{32}$$

to plot $q_m(0)_{exp}$ vs $\epsilon_\chi^{2/3}$. The result gives

$$\epsilon_\chi = \frac{90.65}{\chi_s}\left(\frac{1}{T} - \frac{1}{T_s}\right) \tag{33}$$

with $\chi_s = 0.5356$ and $T_s = 298$ K. We, then, plotted $q_m(0)_{exp}$ as a function of $\epsilon_\chi^{2/3}$ (though we do not show here) and obtained

$$q_m(0)_{exp} = 0.711\epsilon_\chi^{2/3} \tag{34}$$

in unit of nm^{-1}. It is found that the values of $q_m(0)_{exp}$ are smaller than those of $q_m(0)_{theor}$ by a factor of 17.2 for the PS/CH system, indicating that the discrepancy found in PP/CCl_3F is not a unique feature in polymer/suprecritical-fluid systems. Though the origin of the discrepancies is not clear at present, these discrepancies may be due to dynamical asymmetry effects of polymer solutions.[45]

VII. Conclusion

We measured the time changes in the scattered intensity in the early stage SD induced by pressure

jump for PP/CCl_3F. We found that the time changes can be approximated by Cahn linearized theory or CHC theory even though the solution is under nearly supercritical condition. The analyses with the theories yielded the characteristic parameters D_{app} and $q_m(0)$ in the early stage SD. The pressure dependencies of D_{app} and $q_m(0)$ show the mean field behavior, which is different from other experimental results for polymer solutions. This difference was found to be due to the fact that our quench depth is much deeper than those of other experiments. In forthcoming paper, we will analyze the SD processes after the early stage.

References and Notes

(1) Kiran, E. *Supercritical Fluids. Fundamentals for Application*; Kluwer Academic Publishers: Dordrecht, 1994.
(2) Ehrlich, P.; Kurpen, J. J. *J. Polym. Sci.* **1963**, *A1*, 3217.
(3) Saraf, V. P.; Kiran, E. *Polymer* **1988**, *29*, 2061.
(4) Walsh, D. J.; Dee, G. T. *Polymer* **1988**, *29*, 656.
(5) Kiran, E.; Saraf, V. P.; Sen, Y. L. *Int. J. Thermophys.* **1989**, *10*, 437.
(6) Meilchen, M. A.; Hasch, B. M.; McHugh, M. A. *Macromolecues* **1991**, *24*, 4784.
(7) Haschets, C. W.; Shine, A. D. *Macromolecules* **1993**, *26*, 5052.
(8) Kojima, J.; Nakayama, Y.; Takenaka, M.; Hashimoto, T. *Rev. Sci. Instrum.* **1995**, *66*, 4066.
(9) Hashimoto, T.; Kumaki, J.; Kawai, H. *Macromolecules* **1983**, *16*, 641.
(10) Snyder, H. L.; Meakin, P. *J. Chem. Phys.* **1983**, *79*, 5588.
(11) Izumitani, T.; Hashimoto, T. *J. Chem. Phys.* **1985**, *83*, 3694.
(12) Strobl, G. R. *Macromolecules* **1985**, *18*, 558.
(13) Hashimoto, T.; Itakura, M.; Hasegawa, H. *J. Chem. Phys.* **1986**, *85*, 6118.
(14) Kumaki, J.; Hashimoto, T. *Macromolecules* **1986**, *19*, 763.
(15) Takenaka, M.; Izumitani, T.; Hashimoto, T. *Macromolecules* **1987**, *20*, 2257.
(16) Kyu, T.; Saldanha, J. M. *Macromolecules* **1988**, *21*, 1021.
(17) Bates, F. S.; Wiltzius, P. *J. Chem. Phys.* **1989**, *91*, 3258.
(18) Higgins, J. S.; Fruitwala, H. A.; Tomlins, P. E. *Br. Polym. J.* **1989**, *21*, 247.
(19) Kyu, T.; Lim, D.-S. *J. Chem. Phys.* **1991**, *92*, 3944.
(20) Feng, Y.; Han, C. C.; Takenaka, M.; Hashimoto, T. *Polymer* **1992**, *33*, 2729.
(21) Schwahn, D.; Janssen, S.; Springer, T. *J. Chem. Phys.* **1992**, *97*, 8775.
(22) Takenaka, M.; Hashimoto, T. *J. Chem. Phys.* **1992**, *96*, 6177.
(23) Jinnai, H.; Hasegawa, H.; Hashimoto, T.; Han, C. C. *J. Chem. Phys.* **1993**, *99*, 4845.
(24) Jinnai, H.; Hasegawa, H.; Hashimoto, T.; Han, C. C. *J. Chem. Phys.* **1993**, *99*, 8154.
(25) Ying, Q.; Chu, B.; Wu, G.; Linliu, K.; Gao, T.; Nose, T.; Okada, M. *Macromolecules* **1993**, *26*, 5690.
(26) Takenaka, M.; Hashimoto, T. *Macromolecules* **1994**, *27*, 6117.
(27) Chou, Y.; Goldburg, W. I. *Phys. Rev. A* **1979**, *20*, 2105.
(28) Lal, J.; Bansil, R. *Macromolecules* **1991**, *24*, 290.
(29) Kuwahara, N.; Kubota, K. *Phys. Rev. A* **1992**, *45*, 7385.
(30) Kawasaki, K. *Prog.Theor. Phys.* **1977**, *57*, 826.
(31) Koga, T.; Kawasaki, K. *Phys. Rev. A* **1991**, *44*, R817.
(32) Gunton, J. D.; Miguel, M. S.; Sahni, P. S. In *Phase Transitions*; Domb, C., Lebowitz, J. L., Eds.; Academic Press: London, 1983; pp 269−466.
(33) Cook, H. E. *Acta Metall.* **1970**, *18*, 297.
(34) Cahn, J. W. *J. Chem. Phys.* **1965**, *42*, 93.
(35) Koningsveld, R.; Staverman, A. J. *J. Polym. Sci. A-2* **1968**, *6*, 349.
(36) Stein, R. S.; Keane, J. J. *J. Polym. Sci.* **1955**, *13*, 21.
(37) Sato, T.; Han, C. C. *J. Chem. Phys.* **1988**, *88*, 2057.
(38) Stanley, H. E. *Introduction to Phase Transitions and Critical Phenomena*; Oxford University Press: Oxford, 1971.
(39) Kawasaki, K. *Ann. Phys.* **1970**, *61*, 1.
(40) Hashimoto, T. *Phase Transitions* **1988**, *12*, 47.
(41) Schichtel, T. E.; Binder, K. *Macromolecules* **1987**, *20*, 1671.
(42) Brundrup, J.; Immergut, E. H. *Polymer Handbook*; John Wiley & Sons: New York, 1989.
(43) Kurata, M. *Thermodynamics of Polymer Solutions*; Harwood Academic Publishers: New York, 1982.
(44) Fujita, H. *Polymer Solutions*; Elsevier: Amsterdam, 1990.
(45) Doi, M.; Onuki, A. *J. Phys. II (Paris)* **1992**, *2*, 1631.

MA980799N